Article

Contribution of Fluorophore Dynamics and Solvation to Resonant Energy Transfer in Protein-DNA Complexes: A Molecular-Dynamics Study

Massa J. Shoura,[1,2] R. J. K. Udayana Ranatunga,[3] Sarah A. Harris,[5] Steven O. Nielsen,[3] and Stephen D. Levene[1,2,4,*]

[1]Department of Bioengineering, [2]Department of Molecular and Cell Biology, [3]Department of Chemistry, and [4]Department of Physics, University of Texas at Dallas, Richardson, Texas; and [5]Department of Physics and Astronomy, University of Leeds, Leeds, UK

ABSTRACT In Förster resonance energy transfer (FRET) experiments, extracting accurate structural information about macromolecules depends on knowing the positions and orientations of donor and acceptor fluorophores. Several approaches have been employed to reduce uncertainties in quantitative FRET distance measurements. Fluorophore-position distributions can be estimated by surface accessibility (SA) calculations, which compute the region of space explored by the fluorophore within a static macromolecular structure. However, SA models generally do not take fluorophore shape, dye transition-moment orientation, or dye-specific chemical interactions into account. We present a detailed molecular-dynamics (MD) treatment of fluorophore dynamics for an ATTO donor/acceptor dye pair and specifically consider as case studies dye-labeled protein-DNA intermediates in Cre site-specific recombination. We carried out MD simulations in both an aqueous solution and glycerol/water mixtures to assess the effects of experimental solvent systems on dye dynamics. Our results unequivocally show that MD simulations capture solvent effects and dye-dye interactions that can dramatically affect energy transfer efficiency. We also show that results from SA models and MD simulations strongly diverge in cases where donor and acceptor fluorophores are in close proximity. Although atomistic simulations are computationally more expensive than SA models, explicit MD studies are likely to give more realistic results in both homogeneous and mixed solvents. Our study underscores the model-dependent nature of FRET analyses, but also provides a starting point to develop more realistic in silico approaches for obtaining experimental ensemble and single-molecule FRET data.

INTRODUCTION

Förster resonance energy transfer (FRET) has become a commonly used approach in structural molecular biology and biophysics to obtain three-dimensional information about the structure of macromolecules in solution (1–7). Theoretically, FRET occurs through the nonradiative transfer of energy between two fluorophores, namely, an electronically excited donor and a ground-state acceptor. The efficiency of energy transfer, E, is strongly distance dependent and is given by

$$E = \frac{R_0^6}{R_0^6 + R^6} \quad (1)$$

where R is the distance between the fluorophore transition-dipole moments and R_0 is the separation at which E is 50%. R_0 depends on the spectroscopic characteristics of specific donor-acceptor dye pairs and the spatial relationship between fluorophores (8). In principle, given a theoretical value of R_0, Eq. 1 makes FRET a very powerful tool for measuring distances in the range of 1–10 nm (1–6,9–16).

Electronic interactions between the donor and acceptor are normally considered in the weak-coupling limit (17). A number of approximations, including the so-called ideal-dipole approximation (IDA) (18,19), are used to derive a tractable dependence of the energy-transfer rate on the relative orientations of the dye transition-dipole moments (20,21). Nevertheless, independent measurements of the dipole orientation factor, κ^2, are rarely available, which leads to widespread replacement of the actual value of this factor with its isotropically averaged value of 2/3 (22–25). The dependence on κ^2 is embedded in the value of R_0^6, given in nm^6, by

$$R_0^6 = \frac{9\ln(10)\kappa^2\Phi_D J(\lambda)}{128\pi^5 N_{Av}} = 8.79 \cdot 10^{17}\kappa^2 n^{-4}\Phi_D J(\lambda) \quad (2)$$

where Φ_D is the quantum yield of the donor fluorophore, $J(\lambda)$ is the donor-acceptor spectral overlap integral in units of M^{-1} nm^3, N_{Av} is Avogadro's number, and n is the refractive index of the medium, taken to be that of water at 20°C, 1.333, or 1.4 for water/glycerol mixtures at 20°C. The value of κ^2 lies between 0 and 4 and depends on transition-moment dipole orientations through

$$\kappa^2 = [\cos\theta_T - 3\cos\theta_D\cos\theta_A]^2 \quad (3)$$

Submitted August 20, 2013, and accepted for publication June 10, 2014.

*Correspondence: sdlevene@utdallas.edu

Editor: Bert de Groot.

0006-3495/14/08/0700/11 $2.00

http://dx.doi.org/10.1016/j.bpj.2014.06.023

where θ_T is the angle between the donor and acceptor transition dipole vectors, $\vec{\mu}_D$, and $\vec{\mu}_A$, respectively, and θ_D and θ_A are the respective angles $\vec{\mu}_D$ and $\vec{\mu}_A$ make with the vector $\vec{R}$ connecting the centers of the donor and acceptor molecules (see Fig. 1). The value $\kappa^2 = 2/3$ is obtained by spherical averaging over all three of the angles that appear in Eq. 3 (20,22,26,27).

Despite the technique's sensitivity and versatility, the analysis of FRET measurements in terms of macromolecular structure remains a challenge. FRET methods typically involve organic fluorophores conjugated to the molecule(s) of interest. These dyes are often bulky and attached by a linker chain of significant length. Although potential restrictions on dye motions are often acknowledged, the assumption of isotropic fluorophore motions is often used nonetheless. This assumption is invalid in many applications (17,28–30), which can prevent FRET from being used as a truly quantitative technique for accurately measuring inter- or intramolecular distances. In addition to the unknown value of κ^2, other uncertainties militate against determining accurate distances from E and whether temporal or ensemble averaging of κ^2 is appropriate. However, measuring the anisotropy of the donor and acceptor transition-dipole moments sets limits on κ^2 and can significantly reduce uncertainties in the calculated distances (20,22,31,32).

Models based on surface accessibility (SA) are widely used to quantify donor-acceptor geometry in FRET (2,33–35). SA models probe the FRET-dye positions with respect to a static molecular structure of interest. These calculations are based on simple geometric sampling algorithms that approximate the dyes by spheres of a given radius, each connected to the macromolecule by isotropically flexible, but possibly inextensible, linkers. A Monte Carlo (MC) search finds all possible dye positions that do not violate the steric and tethering constraints, thereby defining accessible volumes of presumed uniform density occupied by each dye in the system. The SA values of the transfer efficiency, $<E>$, are subject to many sources of error, including the fact that most dye molecules are not spherical—a steric factor that can contribute to deviations in κ^2 from its isotropic value. Although fluorophore emission anisotropy measurements can reduce uncertainties in κ^2, interpretation of these data requires assumptions about details of fluorophore motion that are difficult to corroborate experimentally (20,22,31).

Errors in $<E>$ also increase if the molecular environment of the dyes affects either the positional or orientational distribution of the transition dipole moments (23,24,28–30,33,36,37). Although molecular-dynamics (MD) simulations are computationally more expensive, they may be more accurate than SA models of fluorescently labeled macromolecules because they provide more detailed insight into fluorophore behavior at the molecular level and can include details such as fluorophore-macromolecule and fluorophore-solvent interactions. A number of studies have employed MD simulations to examine the behavior of dye pairs used in FRET experiments (23,24,28,38–40). Corry and Jayatilaka (38) used atomistic MD simulations to investigate the mobility of fluorophores conjugated to a protein and its effect on FRET efficiency. In another MD study, Iqbal et al. (39) addressed the effects of dye orientation on FRET data analysis, especially in the case of DNA-conjugated cyanine (Cy) dyes. Recently, Hoefling et al. (41) used a fusion of MC and MD techniques to compute statistical distributions of photon bursts and associated single-molecule FRET-efficiency histograms.

In a recent experimental study (42), we used an SA model to interpret ensemble FRET measurements of target-site synapsis in the Cre recombination system. Although that approach did not depend on interpretation of the FRET signal in terms of absolute distances between donor and

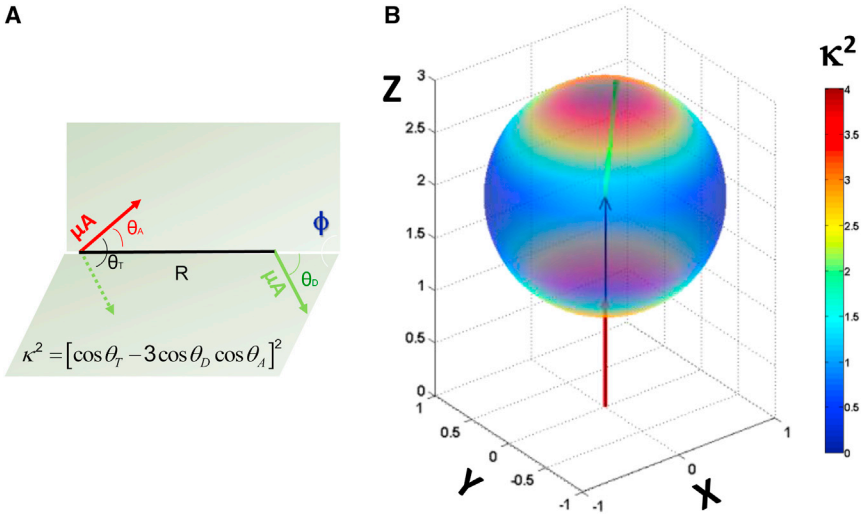

FIGURE 1 (*A*) Geometric definition of the dipole-orientation factor, κ^2, as a function of the spatial relationship between donor and acceptor transition-dipole moments (*green and red arrows*, respectively). (*B*) Three-dimensional heatmap showing the dependence of κ^2 on the polar angle between the donor transition moment and the vector between fluorophore centers of mass, $\vec{R}$. Here, the acceptor transition moment and $\vec{R}$ are coaxial and oriented along the z axis. Under these conditions, κ^2 can take on the full range of possible values from 0 to 4. Two extreme cases can clearly be identified in which the donor and acceptor transition moments are parallel ($\kappa^2 = 4$) or perpendicular ($\kappa^2 = 0$). (Two columns, 6.50″ W × 4.41″ H.) To see this figure in color, go online.

acceptor fluorophores, the experimentally measured E value of the synaptic complex was smaller than expected for isotropically averaged fluorophores tethered to crystallographic models of Cre-recombination intermediates. We concluded in that work that the discrepancy could be due to failure of the isotropy assumption, departure of the synaptic-intermediate conformation from the crystallographic structures, or some combination of these factors.

In this work, we compare an SA analysis of donor/acceptor fluorophore distributions with results obtained from more realistic MD simulations for dye pairs in solution and in Cre recombinase-DNA complexes, which serve as a case study. Our main aim here is to investigate the inherent spatial confinement of a donor-acceptor FRET pair in structures of Cre-DNA synaptic complexes using MD simulations. We assess how this confinement and changes in solvent conditions might affect the interpretation of experimental FRET data in this system, particularly with regard to the effects on dye-distance distributions and deviations from isotropic fluorophore motion on submicrosecond timescales. The motions of the donor and acceptor fluorophores (ATTO 594 and ATTO 647N, respectively) used in Shoura et al. (42) are significantly restricted by the dye-accessible volumes within the intermediate complexes. Such restrictions are less severe in free nucleic acid or peptide studies, where the fluorophores are expected to rotate and diffuse to a significant extent, thereby making the isotropically averaged value of κ^2 more plausible (23). We emphasize that our simulation timescale is not expected to capture large-scale conformational changes in these large protein-DNA complexes.

Specific enzymatic reaction conditions that include significant concentrations of reagents such as glycerol or polyethylene glycol (PEG) may perturb the interactions of the fluorophores with their immediate environment. In this work, we examined the effect of glycerol on dye-distance distributions and κ^2, and hence on distance measurements derived from experimental values of E. It is challenging to maintain adequate conformational sampling in glycerol/water mixtures because of the longer timescale of molecular motion compared with aqueous simulations. Therefore, we used extended trajectories for glycerol/water MD simulations that had up to four times the duration of the corresponding aqueous trajectory (see Table S1 in the Supporting Material). We found that significant concentrations of glycerol substantially altered the balance of dye-dye and dye-macromolecule interactions, leading to dramatic differences between MD and SA dye-distance distributions that were largely uncorrelated with $<\kappa^2>$. Therefore, our results should prompt a more systematic examination of solvent effects on the behavior of conjugated fluorescent probes. This will provide insights that pertain to FRET-data analysis of large systems beyond examples of labeled macromolecules in mixed solvents (43) such as fluorescent micelles and lipids (44).

MATERIALS AND METHODS

System specifications

Four different systems were simulated by MD in the course of this work: 1), donor and acceptor fluorophores tethered to fixed points in space by six-carbon linkers; 2), a DNA duplex bearing the loxP sequence in its standard B-DNA form modeling the product of the Cre-recombination reaction in Shoura et al. (42), where donor and acceptor fluorophores are conjugated to C5 positions of adjacent thymine residues on opposing strands; 3), the Cre Holliday-junction intermediate (HJ) complex based on the PDB cocrystal structure 3CRX (45) with fluorophore labels at sites corresponding to the positions used in Shoura et al. (42); and 4), a fluorophore-labeled Cre-mediated synapse of DNA duplexes based on the PDB cocrystal structure 5CRX (46). In keeping with our effort to replicate the experimental system used in Shoura et al. (42) as closely as possible, we used ATTO 647N as the acceptor fluorophore. The structure of ATTO 594, which was used experimentally as the donor fluorophore, remains proprietary. Therefore, we modeled the donor fluorophore using the known structure of ATTO 610, which shares a common conjugated ring system with the 12 published ATTO-dye structures. The isotropic value of R_0, $R_{0,iso}$, for the ATTO 610/647N donor-acceptor pair is 7.3 nm, which is closely comparable to that for the ATTO 594/647N pair (7.5 nm). Finally, we replaced the noncanonical DNA sequence in the lox recombination-site spacer of 3CRX to regenerate the wild-type loxP target site.

MD simulation protocol

Simulations were carried out using the NAMD software package (47) with force-field parameters based on the CHARMM libraries (48). CHARMM 27 parameters were used for nucleic acid and protein moieties, whereas new topology files were created for the fluorophores (ATTO 610/647N) as well as the six-carbon linker chain that connects the fluorophores to the C5 positions of specific thymine residues (see Fig. 2).

Simulation details

In vacuo simulations were run using Langevin dynamics at 300 K under isochoric conditions. Simulations of solvated systems used the TIP3P water

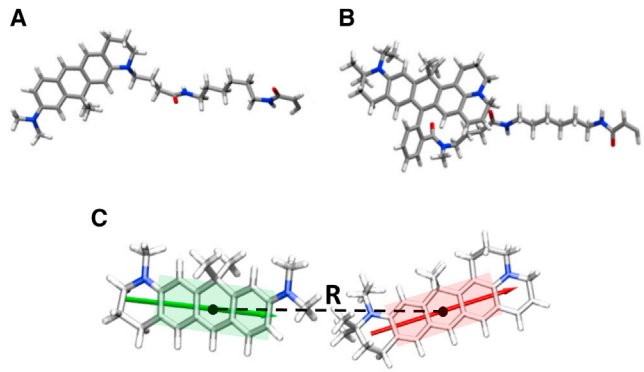

FIGURE 2 Molecular structures of the fluorophores used in this work. (*A*) Canonical structure of the donor, ATTO 610, conjugated to a C-6 linker. (*B*) Structure of the acceptor dye, ATTO 647N, attached to the same linker shown in (*A*). (*C*) Geometry-optimized structures of fluorophore ring systems corresponding to the donor excited state and acceptor ground state obtained from ab initio quantum-mechanical calculations. The directions of the transition-dipole moments are indicated (*arrows*). We define R as the distance between the centers of mass of rigid three-ring conjugated systems corresponding to each dye. (One column; 3.25″ W × 2.34″ H.) To see this figure in color, go online.

model and a constant pressure of 1 atm was maintained using a Nose-Hoover-Langevin piston (49). A time step of 2 fs was used in all simulations in conjunction with the RATTLE/SHAKE algorithm to constrain the bonds between hydrogen and heavy atoms at their equilibrium distances during the dynamics. A nonbonded cutoff of 1.2 nm with a smooth switching function between 1.0 nm and 1.2 nm was used for van der Waals interactions and the short-ranged component of the electrostatic interactions, whereas long-ranged electrostatic interactions were treated using the particle-mesh Ewald method. Pair-neighbor lists were maintained for particles within 1.35 nm of one another.

Simulation procedure and data analysis

Simulations containing protein and/or DNA were performed in three stages. In the first stage, short (~1 ns) simulations were run in which the atomic positions of the polypeptide and/or nucleic acid backbones were constrained to their initial positions using a soft harmonic constraint of the form

$$U\left(\vec{q}\right) = k_H\left(\vec{q} - \vec{q}_{ref}\right)^2 \quad (4)$$

where k_H is a harmonic force constant, $\vec{q}$ is the position of a constrained atom, and $\vec{q}_{ref}$ is the initial (reference) position. The value of k_H was set at 5 kcal mol^{-1} Å^{-2}. In the second stage, the system was allowed to relax with constraints applied only to the terminal basepairs of the DNA structures; this prevents the terminal residues from acting as free ends, which is not the case in experiments. In the third stage, longer simulation times were used. Data were collected only from the third stage of each simulation, where constraints were maintained on the terminal basepairs of the DNA and the systems were taken to be at thermodynamic equilibrium. The minimum trajectory duration exceeded 35 ns for all simulation results reported here.

To monitor the convergence of trajectories for all systems simulated in this study (see Table S1), we used several methods, including block averaging and autocorrelation analysis. Block-averaging analysis consists of reblocking the apparent standard error (SE), σ, of the time average of κ^2, $<\kappa^2(t)>_T$, as a function of time over the duration of a given trajectory (50). Here, $<f(t)>_T$ denotes $1/T\int_0^T f(t)dt$, where T is the duration of a trajectory. Block-size-dependent values, σ_j, are computed sequentially using block sizes of $j = 3, 4, 5,\ldots, N$ frames with N the total number of frames in a trajectory. An estimate of the SE in $<\kappa^2(t)>_T$ for the complete trajectory, σ^*, is obtained by fitting σ_j as a function of j to an exponential growth curve as shown in Fig. S1. This method, though straightforward, leads to a lower bound for σ^* and is limited by the size of the data set. The dependence of σ_j on j is not expected to approach a finite value σ^* if the parameter distribution is not equilibrated. Although we could have run multiple simulations of the same DNA-Cre system using different initial positions for the dyes as a test for convergence, in principle, the ATTO dyes are bulky substituents and are not arbitrarily accommodated within the structure of the protein-DNA complex. As a result, we could not generate two significantly different initial configurations of dyes within the core of the Cre-HJ complex without seriously violating steric and geometric constraints.

We used the dye positions and orientations to compute the time-dependent anisotropy (40), $r(\tau) = 2/5<P_2[\vec{\mu}(t)\cdot\vec{\mu}(t+\tau)]>_T$, where $\vec{\mu}(t)$ is the transition dipole moment at time t and P_2 is the second Legendre polynomial, as well as the autocorrelation function for κ^2, $C(\kappa^2,\kappa^2;\tau) = <\kappa^2(t)\,\kappa^2(t+\tau)>_T$ (Figs. S2 and S3). We compared time-averaged dynamic quantities computed from the trajectories, $<f(t)>_T$, with ensemble averages of the same quantities taken over all configurations of the system, $<f>$. In the limit of an ergodic system in which both the time T and number of systems in the ensemble are arbitrarily large (a condition that is virtually never met in computer simulations), $<f(t)>_T$ and $<f>$ are identically equal (51). In the ergodic limit, this equivalence extends to the corresponding experimental quantity, which we specify in our notation by dropping the angle brackets (e.g., the theoretical FRET efficiency $<E(t)>_T \simeq <E>$ asymptotically approaches the experimental value, E).

Structure and parameterization of the fluorophores

We assigned the atomic partial charges on the ATTO dyes using the CHARMM convention for all atoms other than nitrogen and atoms belonging to the fluorophore structures. We determined the charges for these atoms by scaling the fitted electrostatic potential (ESP) charges from ab initio quantum-mechanical calculations described below, making sure to conserve the total charge. The equilibrium values of bond lengths and angles were either taken directly from the CHARMM force field for known interactions or iteratively adjusted to match values from ab initio geometry-optimized structures (see below). Force constants for bond stretching and bond-angle displacement were largely assigned by analogy with existing parameters in the CHARMM 27 force field. When suitable parameters were not available from the CHARMM force field, the fully compatible CGenFF force-field parameters were used instead. Parameters for the bond torsions and nonbonded interactions were found in a similar manner.

We note that force-field parameterization may play a considerable role in the observed behavior of the dyes. It is presently unknown what level of theory is necessary to accurately model dye behavior; for example, approaches under development involving polarizable force-field terms (52) or mixed quantum-/molecular-mechanics approaches (53) may give more realistic behavior. Also, interaction parameters that are generated automatically using standard software packages are not always accurate; for example, such parameters do not always capture the aromaticity of conjugated atoms. For the calculations in this work, we checked the final dye parameters against those that were automatically generated through the ParamChem interface and found them to be in good agreement. Detailed force-field parameters for the ATTO dyes are given in topology-file format as an Appendix in the Supporting Material.

Ab initio quantum-mechanical calculations

Hartree-Fock quantum calculations were carried out on the conjugated portions of the donor and acceptor fluorophores that comprised the planar ring system of each dye (38). An initial conformational search was implemented using the OPLS molecular-mechanics force field prior to geometry optimization using a 6-31G** basis set. Single-point calculations were carried out from these structures using a 6-31+G** basis set and were used to fit the ESP charges to atomic nuclei. In addition, CIS evaluations were implemented to find the transition-dipole moments of the dyes (see Fig. 2). All ab initio calculations were carried out using the Jaguar software package by Schrödinger (Portland, OR).

Stability of simulated systems

We monitored the van der Waals and electrostatic components of protein-protein and protein-DNA interaction energies in the modified 3CRX structure modeled in these simulations. These calculations were done with and without conjugated dyes. The interaction-energy values serve two main functions: 1), to provide one of several internal checks on the validity of the simulation; and 2), to ensure that the conjugated dyes do not strongly destabilize the 3CRX complex. The results show that there are negligible differences in the total protein-protein and protein-DNA interaction energies for dye-labeled and unlabeled complexes (Fig. S4).

Simulations in glycerol/water mixed-solvent systems

Because of the complexity of simulating a Cre-DNA complex suspended in the actual components of the buffer used in Shoura et al. (42), we chose to approximate the experimental buffer system by using a glycerol/water mixture with a bulk dielectric-constant value similar to that of the

experimental buffer. We generated a single, large solvent box containing only the glycerol/water mixture by combining two smaller homogeneous boxes of each component and allowing the solvents to equilibrate (54). Two previously equilibrated simulation cells with dimensions 7.5 × 7.5 × 7.5 nm^3, each containing 0.2 M NaCl in either water or glycerol, were merged to obtain a large solvent box of size 15 × 7.5 × 7.5 nm^3. The mole fraction of glycerol was 0.39 (2796 glycerol and 4428 water molecules), which approximates that of the nonaqueous components in some experimental Cre-recombination buffers (42,55). We verified that the concentrations of the two solvents were spatially uniform before introducing the solutes. Solvation was performed by superimposing the solute and mixed-solvent simulation boxes; solvent molecules having atoms within 0.15 nm of solute atoms were discarded.

RESULTS AND DISCUSSION

Dynamics of tethered ATTO dye pairs

We carried out a series of simulations on solvated donor/acceptor dye pairs in which each dye molecule was tethered by its linker to a fixed point in space (Fig. 3). The tethering points were separated by a distance d along the long central axis of the simulation cell, and the through-space distance between dye centers of mass, R, and the orientation factor, κ^2, were monitored for these trajectories. These simulations had the following objectives: 1), to confirm that $<\kappa^2>$ approaches its isotropic value of 2/3 for dyes without restricted rotation; 2), to estimate the minimum length of a trajectory needed to equilibrate the system with respect to sampling of dye orientations; and 3), to investigate the dependence of κ^2 on R in aqueous and glycerol/water solvent systems.

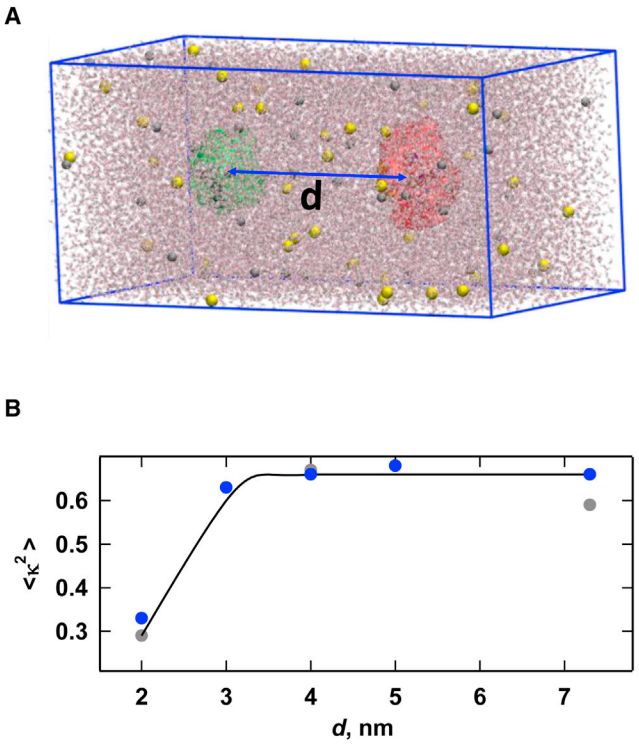

FIGURE 3 (*A*) Typical simulation of tethered linker-conjugated fluorophores. A snapshot of a particular configuration of water molecules and ions (0.2 M NaCl; Na^+ in *gray*, Cl^- in *yellow*) is superimposed on the donor (*green*) and acceptor (*red*) positions integrated over the course of a 40-ns trajectory. Values of the tethering distance, d, were varied from 2 nm to 7.3 nm (shown). (*B*) Dependence of $<\kappa^2(t)>_T$ on d for MD simulations in aqueous and glycerol/water solvent systems; the continuous curve is merely a guide for the eye. Note that $<\kappa^2(t)>_T$ assumes the isotropic value of 2/3 for all but the smallest value of d (2.0 nm). (One column, 3.25″ W × 3.10″ H.) To see this figure in color, go online.

Over the range of $d = 3.0$–7.3 nm, $<\kappa^2(t)>_T$ was found to be 0.66 ± 0.04, which is essentially identical to the isotropically averaged value of 2/3 in both aqueous and glycerol/water simulations. However, this was not the case for $d =$ 2.0 nm, where $<\kappa^2\ (t)>_T = 0.33$ for aqueous simulations and 0.29 for glycerol/water. This pronounced decrease in $<\kappa^2(t)>_T$ in both solvents is likely due to the increasing strength of dye-dye interactions with decreasing values of d (discussed below) rather than a failure of the system to reach equilibrium.

Short-range interactions similarly affected the relaxation behavior of $C\ (\kappa^2, \kappa^2, \tau)$ for $d = 2.0$ nm, which converged weakly relative to data for larger values of d. For $d \geq$ 3 nm, $C\ (\kappa^2, \kappa^2, \tau)$ gave single-exponential decay times between 100 and 175 ps (Fig. S2). These relaxation times are semiquantitatively consistent but slightly larger than those obtained by Deplazes et al. (40) for untethered Alexa dyes, which have smaller ring systems than the dyes examined in this study. As noted in Materials and Methods, force-field parameterization is a critical determinant of simulation accuracy in any MD study. At present, standard parameterization techniques, such as those used here, do not fully take into account important phenomena such as molecular polarizability. The dye dynamics observed here are reassuringly consistent with previous results; however, it remains to be shown that a similar consistency holds in the case of more sophisticated parameterization schemes.

Also, there appears to be a negligible cross correlation of R and κ^2 (Fig. S3), which validates the use of Eq. 2 as discussed in Deplazes et al. (40). The relaxation times for $C\ (\kappa^2, \kappa^2, \tau)$ are significantly smaller than the anisotropy decay times of individual dyes in the tethered-dye simulations, which are in the range of 500 ps in water and 1.5 ns in glycerol/water (Fig. S5). The dependence of anisotropy decay times on solvent conditions exactly follows the increment in bulk solvent viscosity (56).

Solvent effects on the tethered fluorophore-linker conformation

Linker groups tethering the fluorophores are expected to be highly flexible. Nonetheless, we find that dye-linker interactions can potentially restrict fluorophore motion. The structure of the ATTO 610/linker moiety in aqueous simulations with $d = 4.0$ nm alternated between the two conformations shown in Fig. 4, i.e., a fully extended form and a U-shaped

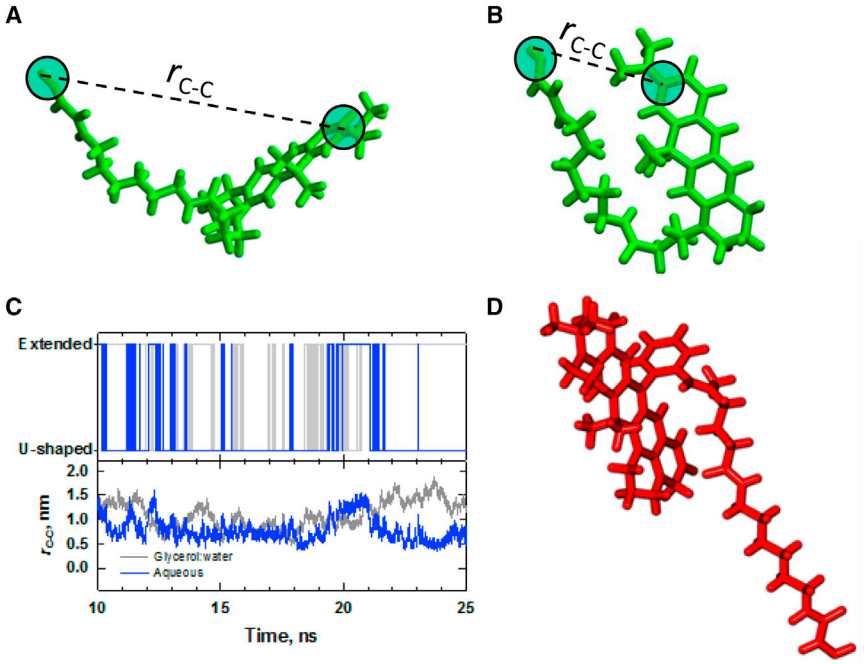

FIGURE 4 Conformational states of linker-conjugated fluorophores. (*A*) Extended and (*B*) U-shaped conformations of the ATTO 610-linker conjugate. This conformational equilibrium can be characterized by examining fluctuations of the distance between the designated carbon atoms, r_{C-C}. (*C*) Behavior of r_{C-C} over a 15 ns window in aqueous (*blue*) and glycerol/water (*gray*) simulations. The lower panel shows the actual time dependence of r_{C-C}, and the upper panel is the result of a binary classifier applied to the continuous r_{C-C} distribution. Here, the dye/linker conformation was scored as extended if $r_{C-C} \geq 1$ nm and U-shaped otherwise. (*D*) Time-averaged structure of linker-conjugated ATTO 647. (Two columns, 6.50″ W × 5.24″ H.) To see this figure in color, go online.

conformation. Because this tethering distance is large enough for the dyes to exert a minimal influence on each other, the U-shaped conformation may possibly be stabilized by hydrophobic interactions between the dye and linker. Aqueous conditions slightly favor the U shape (56:44 U-shaped: extended), whereas solvation in glycerol/water inverts this ratio (44:56 U-shaped: extended). This difference in conformational bias evidently has negligible effects on $<\kappa^2(t)>_T$, which had similar values for both solvents (Fig. 3 *B*). The ATTO 647N linker was predominantly folded into the hairpin structure shown in Fig. 4 *D* independently of the solvent conditions. This is probably due to the sterically preferred orthogonal orientation of the linker-conjugated, six-membered ring relative to the plane of the main hexacyclic group in the fluorophore (see Movie S1).

Pair-distance distributions for tethered fluorophores

This MD study was motivated in part by the previous use of simplified models for calculating spatial distributions of fluorophores based on SA (34,35). As discussed above, SA models contain many assumptions, not the least of which is that the dyes interact with one another and with macromolecular components only through hard-sphere repulsive interactions. Possible attractive forces between dyes and other species are not normally considered. We hypothesized that these assumptions needed verification, especially in the case of experiments where details of dye-dye interactions might be altered by solvation conditions.

Previous Cre-mediated DNA synapsis experiments used mixed-solvent buffer conditions to obtain measurable levels of intermolecular Cre recombination (42). The buffer in question consists of 25 mM N-Tris[hydroxymethyl] methyl-3-aminopropanesulfonic acid (TAPS), 180 mM NaCl, and 2 mM $MgCl_2$ plus significant concentrations of glycerol, PEG, and bovine serum albumin (BSA) (55). It is not practical to introduce additional high-molecular-weight species such as PEG and BSA into simulations of systems as large as a Cre-DNA synapse; thus, we sought to approximate the effect of these species on the buffer dielectric constant in the simulation by using a binary mixture of glycerol and water as the solvent. This mixture, which has a glycerol mole fraction of 0.39, yields a bulk dielectric constant similar to that of the original buffer solution used in the recombination experiments (42,55). We compensated for the longer dye correlation times in glycerol/water relative to aqueous conditions (see above) by extending the duration of the mixed-solvent trajectories well beyond those of corresponding aqueous simulations. Thus, the minimum duration of the glycerol/water trajectories for any of the systems studied here was 100 ns.

We found radical differences in the dye-pair distance-distribution functions obtained for MD simulations of tethered fluorophores carried out in water and in glycerol/water, as shown in Fig. 5. Notably, none of the MD distributions bore any resemblance to the near-Gaussian distribution computed using an MC-based SA calculation as described in Shoura et al. (42). Whereas a clear propensity for the dyes to form attractive interactions exists in the aqueous case, there is a measureable tendency for the dyes to repel each other in water/glycerol. Such effects are not taken

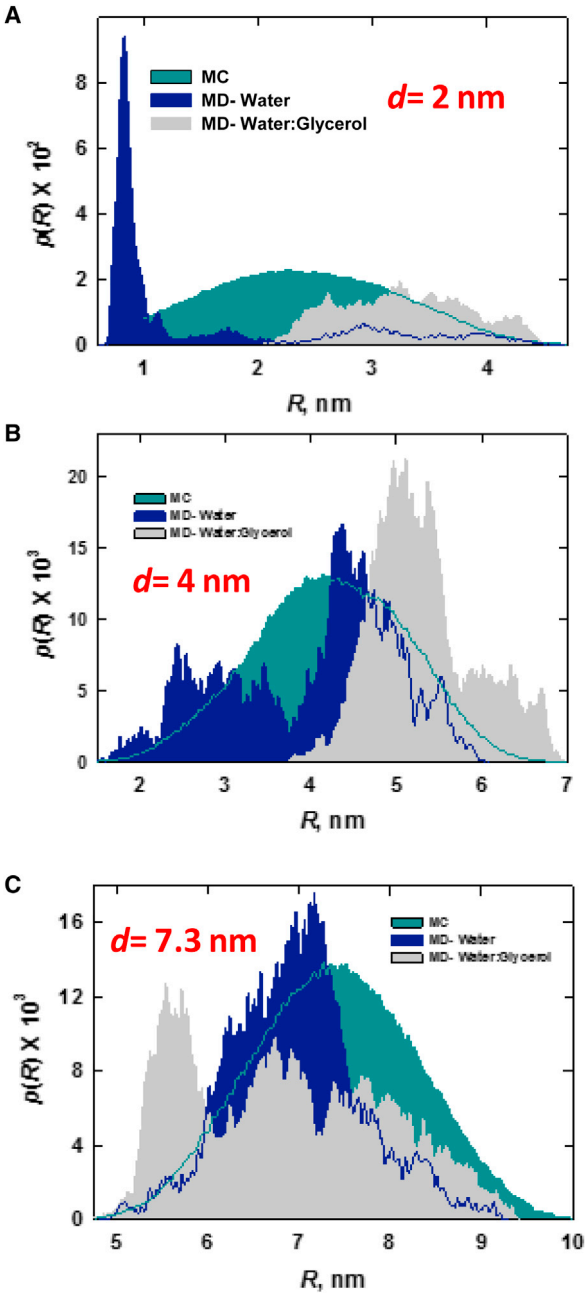

FIGURE 5 Dye-pair distance-distribution functions for tethered fluorophores as a function of d in aqueous (*blue*) and glycerol/water (*gray*) MD simulations. Results of MC SA calculations are shown for comparison in green. Post hoc statistical analysis using the ANOVA/Tukey method yields $p < 0.05$ for pairwise comparisons of all of the distributions in A and B. Based on this analysis, we can conclude that the differences in SA, MD (aqueous), and MD (glycerol/water) distance distributions for tethered ATTO dyes where $d \leq 4$ nm are statistically significant. Differences in the distributions in C, where $d = 7.3$ nm, are not statistically significant, $p = 0.48$). (One column, 3.25″W × 6.95″H.) To see this figure in color, go online.

into account in the MC model; moreover, solvent effects are present in the simulation over a range of separations, d, from 2.0 nm to at least 4.0 nm. The most plausible explanation for the solvent dependence is that dye-dye interactions are mainly driven by hydrophobic forces in aqueous media. The reduced dielectric shielding in glycerol/water mixtures increases the strength of charge-charge interactions. Because both dyes have a single negative charge under these simulation conditions, Coulombic interactions became the dominant force, leading to a net dye-dye repulsion that is not observed in the aqueous case.

The dependence of $<R(t)>_T$, $<\kappa^2(t)>_T$, and $<E(t)>_T$ as a function of tethering distance d is shown for both solvents and also compared with MC values for $<R>$ and $<E>$ in Fig. 6. Note that $<E(t)>_T$ is computed from values of $R(t)$ and $\kappa^2(t)$ for each frame. Although this approach is not rigorously correct due to conformational fluctuations that can occur during the lifetime of the donor excited state (41,57), it permits comparisons between a model that takes into account detailed interactions on the atomic scale with simple SA-based models.

As discussed above, the value of $<\kappa^2>$ is not dramatically affected by solvent conditions; we find that $<\kappa^2>$ assumes its isotropic value of 0.67 for all but the smallest value of

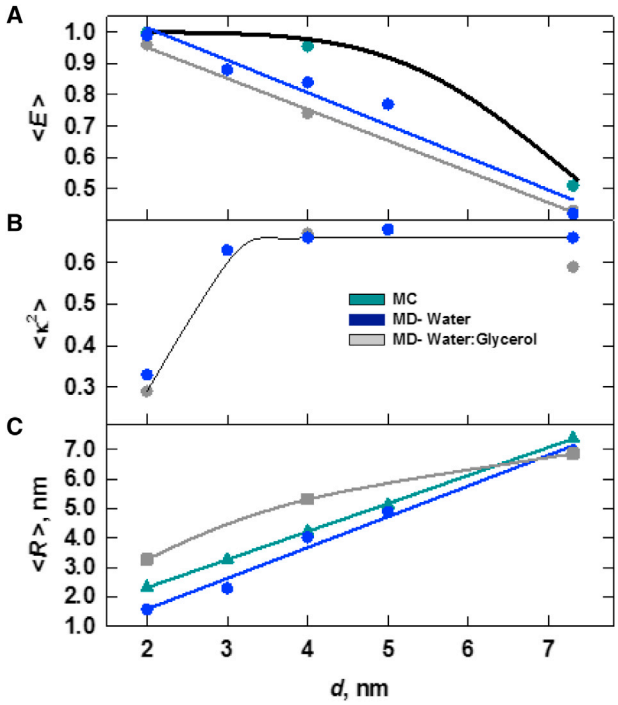

FIGURE 6 Behavior of $<R(t)>_T$, $<\kappa^2(t)>_T$, and $<E(t)>_T$ for tethered ATTO dyes as a function of distance d in aqueous (*blue data points*) and glycerol/water (*gray data points*) MD simulations and for the SA model (*green data points*). The dependence of $<E(t)>_T$ on R (Eq. 1, *black curve*) for $R_0 = 7.3$ nm is in good agreement with the SA data. The middle panel gives the dependence of $<\kappa^2(t)>_T$ on d for MD simulations in aqueous and glycerol/water solvent systems; these data are identical to those in Fig. 3 *B*. The bottom panel shows the dependence of $<R(t)>_T$ on d. For large values of d ($d = 7.3$ nm), the effects of solvent on $<R(t)>_T$ and $<E(t)>_T$ are negligible. Error bars corresponding to ±1 SE are smaller than the data points. (One column, 3.25″ W × 3.89″ H.) To see this figure in color, go online.

d investigated (Fig. 6, *middle panel*). However, there is a systematic trend in the average through-space separation of the dyes, $<R>$, which is reflected in the computed energy-transfer efficiency $<E>$. Being largely hydrophobic, interactions of the dye with the less-polar solvent are favored, accompanied by attenuated dye-dye interactions.

For the case in which $d = 4.0$ nm (Fig. 6 *B*), $<R>$ for glycerol/water simulations is significantly larger than the value of $<R>$ obtained in aqueous conditions, leading to a reduction in $<E>$ from 0.84 to 0.74. We also note that in the regime where $<\kappa^2>$ deviates significantly from 0.67, $<E>$ is highly insensitive to $<\kappa^2>$. This is expected to be true for most systems in which the average dye-dye distance is small compared with the isotropic value of R_0.

Rotational dynamics of dyes conjugated to DNA and protein-DNA complexes

We carried out MD simulations on protein-DNA complexes based on crystallographic structures available for the Cre antiparallel synapse (PDB: 5CRX) and the Cre-HJ (PDB: 3CRX). Three different DNA structures (loxP duplex, system 2), Cre-loxP synapse (system 3), and Cre-loxP HJ (system 4) (see Fig. 7) were simulated with dyes conjugated to positions corresponding to the locations of the donor and acceptor fluorophores in the putative intermediates and recombination product generated in Shoura et al. (42). Furthermore, we took the mechanistic cleavage-pattern distribution of Cre (58) into account by investigating two distinct strand-cleavage scenarios for each of the Cre synapse and HJ structures. Based on previous experimental studies (45,46,58), we expect that 80% of the complexes are scenario 1 (GC-cleavage) complexes. A minority (20%) of complexes are generated via AT cleavage, which we denote the scenario 2 complex (58). Table 1 shows that the $<\kappa^2>$ value for conjugated dyes in all of these models deviates from the isotropic value of 2/3. This is clearly due to the restricted mobility of the conjugated ATTO dyes, which is also the case for the duplex DNA recombination product (24,39).

Differences between MD and experimental FRET efficiencies for the Cre-HJ complex

Previous studies support the notion that the Cre-HJ intermediate is the longest-lived intermediate in the Cre recombination pathway (42,55,59). We therefore focused on the solvent dependence of dye dynamics in the HJ Cre-DNA (PDB: 3CRX) structure. Fig. 8 shows the MD dye-distance distributions for the labeled HJ Cre-DNA complex in water and glycerol/water along with the MC-simulated distribution for the same structure. Clearly, the MD distributions obtained for both solvent systems are radically different from the MC results. Moreover, the same trend in the solvent-dependent MD distance distributions observed in the case of tethered dyes, namely, a larger value of $<R>$ in glycerol/water versus aqueous 0.2 M NaCl, is recapitulated here. Thus, we conclude that repulsive forces between the ATTO dyes dominate the dye-distance distribution in glycerol/water even within the highly restricted environment of the protein-bound HJ. By comparing the present simulation results with experimental results reported in Shoura et al.

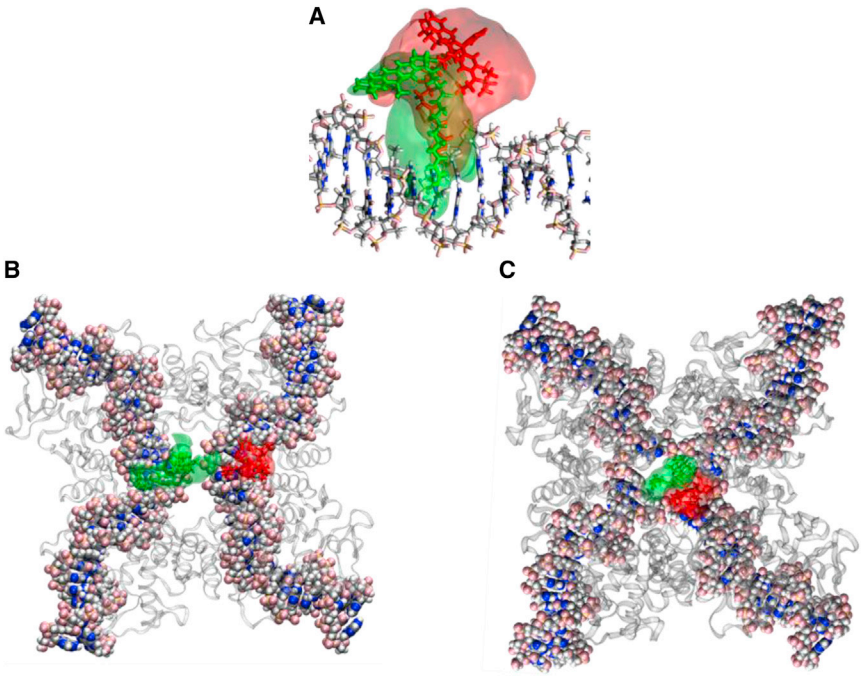

FIGURE 7 ATTO-DNA systems simulated by MD in the course of this work. (*A*) DNA duplex modeling the product of the Cre-recombination reaction in (42), in which donor and acceptor fluorophores are conjugated to C5 positions of adjacent thymine residues on opposing strands. (*B*) A fluorophore-labeled Cre-mediated synapse of DNA duplexes based on the PDB cocrystal structure 5CRX (46,60). (*C*) The Cre HJ intermediate complex based on the PDB cocrystal structure 3CRX (45,46,60) with fluorophore labels at sites corresponding to the positions used in Shoura et al. (42). Integrated positions of donor (*green*) and acceptor (*red*) centers of mass over the course of complete trajectories in aqueous solution are shown. See also Movie S2. (Two columns, 6.5″ W × 5.19″ H.) To see this figure in color, go online.

TABLE 1 Values of $<\kappa^2(t)>_T$ and $<E(t)>$ for different MD simulations in this study

System	Solvent	$<\kappa^2(t)>_T$, ($\pm$ σ^*)	$<E(t)>$
5CRX: antiparallel Cre-DNA synaptic complex	aqueous	0.71 ($\pm$ 0.13)	0.98
5CRX: parallel Cre-DNA synaptic complex	aqueous	1.17 ($\pm$ 0.16)	0.98
3CRX: Cre-DNA Holliday junction intermediate (scenario 1)	aqueous	0.28 ($\pm$ 0.03)	0.99
3CRX: Cre-DNA Holliday junction intermediate (scenario 1)	water/glycerol	0.12 ($\pm$ 0.02)	0.96
3CRX: Cre-DNA Holliday junction intermediate (scenario 2)	aqueous	0.70 ($\pm$ 0.12)	0.99
LoxP duplex	aqueous	0.36 ($\pm$ 0.04)	0.99

Lower-bound uncertainties, which were obtained by block averaging (see Fig. S1), are given as ± 1 SE ($\pm\sigma^*$).

(42) for the Cre synaptic complex ($E = 0.88$), we find that the relative reduction in $<E>$ for glycerol/water (0.96) versus aqueous MD simulations (0.99) amounts to about half of the discrepancy between the experimental E (0.88) and the SA/MC value of 0.99 expected for isotropically averaged fluorophores tethered to the crystallographic Cre-HJ intermediate.

This small but possibly significant difference (see Fig. 8) points to a potential role of solvent conditions in attenuating energy transfer between dyes. However, we cannot completely rule out the possibility that other factors that were not captured by the MD simulations may have contributed to the experimentally observed E value. These include

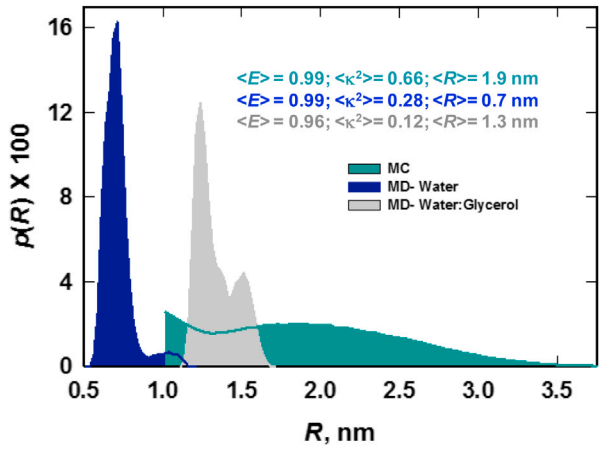

FIGURE 8 Distance distributions for fluorophores in the DNA-Cre HJ (see Fig. 7 *C*). The MD distributions were computed from aqueous (*blue*) and glycerol/water (*gray*) MD simulations; MC SA results are shown in green. The cutoff in the SA results at 1 nm is due to the treatment of donor and acceptor dyes as 1-nm-diameter hard spheres. Post hoc ANOVA/Tukey statistical analysis of pairs of distributions gave confidence intervals of $p < 0.05$ for all pairs, indicating that differences among the distributions are statistically significant. (One column, 3.25″ W × 2.47″ H.) To see this figure in color, go online.

geometric distortion of the Cre-HJ intermediate relative to its crystallographic structure and/or differences between the proxy dye ATTO 610 and the actual dye used in the experiments (ATTO 594). Thus, a reevaluation of the solvent-dependent interactions between donor and acceptor may be needed when the ATTO 594 structure becomes available. Finally, trajectories approaching a 200 ns duration, which are limited by the size of these systems, are likely still far short of the timescale that is involved in conformational rearrangements of the complex.

CONCLUSIONS

Under the right conditions, the distance dependence of energy transfer in FRET experiments is a powerful tool for investigating macromolecular structure and interactions. When donor-acceptor dye pairs are sufficiently close to one another ($R << R_0$), FRET is a reliable reporter of probe-probe proximity because energy transfer depends weakly on the orientation factor, κ^2. We exploited this lack of sensitivity in previous studies of the Cre-loxP recombination system (42), in which we used FRET as a binary reporter of the probe-pair distance.

It is challenging to interpret measured energy-transfer efficiency values in terms of fluorophore-fluorophore distances in an intermediate distance regime, not least because of common failure of the isotropic rotation assumption. Many modeling approaches for estimating $<R>$ from $<E>$ rely on probe distributions computed from SA (2,33–35). However, our work suggests that when taking realistic dye properties into account, one should consider that the dye-dye, dye-solvent, and dye-macromolecule interactions make significant contributions to the spatial and orientational distributions of these probes. This conclusion suggests that the use of realistic MD-based modeling incorporating details such as solvent composition can be a powerful adjunct to experimental design strategies for choosing the location and chemical environment of fluorescent probes in future FRET studies. Indeed, it is possible that the FRET experiments in Shoura et al. (42) could have been more highly optimized to extract structural information about the Cre synaptic complex if MD-based modeling results had been available in advance. Ideally, iterative cycles of simulation, experimental design, and laboratory measurements can be a highly effective approach for FRET-based studies of complex macromolecular structures.

SUPPORTING MATERIAL

Five figures, one table, one appendix and two movies are available at http://www.biophysj.org/biophysj/supplemental/S0006-3495(14)00663-8.

We thank Stefan Giovan and Blake Wilson for helpful discussions. The use of the High-Performance Computing resources of the Texas Advanced Computing Center at The University of Texas at Austin is gratefully acknowledged.

This work was supported by grants from the National Institutes of Health /National Science Foundation Joint Program in Mathematical Biology (DMS-0800929 to S.D.L.), the SRC Engineering Research Center (to S.O.N.), and the UK Biotechnology and Biological Sciences Research Council (BB/1019294/1 to S.A.H.).

REFERENCES

1. Mitra, R. D., C. M. Silva, and D. C. Youvan. 1996. Fluorescence resonance energy transfer between blue-emitting and red-shifted excitation derivatives of the green fluorescent protein. *Gene.* 173:13–17.
2. Treutlein, B., A. Muschielok, …, J. Michaelis. 2012. Dynamic architecture of a minimal RNA polymerase II open promoter complex. *Mol. Cell.* 46:136–146.
3. Day, R. N. 1998. Visualization of Pit-1 transcription factor interactions in the living cell nucleus by fluorescence resonance energy transfer microscopy. *Mol. Endocrinol.* 12:1410–1419.
4. McKinney, S. A., A. D. Freeman, …, T. Ha. 2005. Observing spontaneous branch migration of Holliday junctions one step at a time. *Proc. Natl. Acad. Sci. USA.* 102:5715–5720.
5. Tan, E., T. J. Wilson, …, T. Ha. 2003. A four-way junction accelerates hairpin ribozyme folding via a discrete intermediate. *Proc. Natl. Acad. Sci. USA.* 100:9308–9313.
6. Bussiek, M., K. Tóth, …, J. Langowski. 2006. Trinucleosome compaction studied by fluorescence energy transfer and scanning force microscopy. *Biochemistry.* 45:10838–10846.
7. Singleton, S. F., and J. Xiao. 2001-2002. The stretched DNA geometry of recombination and repair nucleoprotein filaments. *Biopolymers.* 61:145–158.
8. Förster, T. 1949. Experimental and theoretical investigation of the intermolecular transfer of electronic excitation energy. *Z. Naturforsch. A.* 4:321–327.
9. Miick, S. M., R. S. Fee, …, W. J. Chazin. 1997. Crossover isomer bias is the primary sequence-dependent property of immobilized Holliday junctions. *Proc. Natl. Acad. Sci. USA.* 94:9080–9084.
10. Wozniak, A. K., G. F. Schröder, …, F. Oesterhelt. 2008. Single-molecule FRET measures bends and kinks in DNA. *Proc. Natl. Acad. Sci. USA.* 105:18337–18342.
11. Margittai, M., J. Widengren, …, C. A. Seidel. 2003. Single-molecule fluorescence resonance energy transfer reveals a dynamic equilibrium between closed and open conformations of syntaxin 1. *Proc. Natl. Acad. Sci. USA.* 100:15516–15521.
12. Ha, T., A. G. Kozlov, and T. M. Lohman. 2012. Single-molecule views of protein movement on single-stranded DNA. *Annu. Rev. Biophys.* 41:295–319.
13. Tomschik, M., K. van Holde, and J. Zlatanova. 2009. Nucleosome dynamics as studied by single-pair fluorescence resonance energy transfer: a reevaluation. *J. Fluoresc.* 19:53–62.
14. Bönisch, C., K. Schneider, …, S. B. Hake. 2012. H2A.Z.2.2 is an alternatively spliced histone H2A.Z variant that causes severe nucleosome destabilization. *Nucleic Acids Res.* 40:5951–5964.
15. White, C. L., and K. Luger. 2004. Defined structural changes occur in a nucleosome upon Amt1 transcription factor binding. *J. Mol. Biol.* 342:1391–1402.
16. Gell, C., T. Sabir, …, P. G. Stockley. 2008. Single-molecule fluorescence resonance energy transfer assays reveal heterogeneous folding ensembles in a simple RNA stem-loop. *J. Mol. Biol.* 384:264–278.
17. Muñoz-Losa, A., C. Curutchet, …, B. Mennucci. 2009. Fretting about FRET: failure of the ideal dipole approximation. *Biophys. J.* 96:4779–4788.
18. Chang, J. C. 1977. Monopole effects on electronic excitation interactions between large molecules. I. Applications to energy transfer in chlorophylls. *J. Chem. Phys.* 67:3901.
19. Krueger, B. P., G. D. Scholes, and G. R. Fleming. 1998. Calculation of couplings and energy transfer pathways between the pigments of LH2 by the ab initio transition density cube method. *J. Phys. Chem. B.* 102:5378–5386.
20. Dale, R. E., J. Eisinger, and W. E. Blumberg. 1979. The orientational freedom of molecular probes. The orientation factor in intramolecular energy transfer. *Biophys. J.* 26:161–193.
21. Badali, D., and C. C. Gradinaru. 2011. The effect of Brownian motion of fluorescent probes on measuring nanoscale distances by Förster resonance energy transfer. *J. Chem. Phys.* 134:225102.
22. Dale, R. E., and J. Eisinger. 1974. Intramolecular distances determined by energy transfer. Dependence on orientational freedom of donor and acceptor. *Biopolymers.* 13:1573–1605.
23. Allen, L. R., and E. Paci. 2009. Orientational averaging of dye molecules attached to proteins in Förster resonance energy transfer measurements: insights from a simulation study. *J. Chem. Phys.* 131:065101.
24. Ouellet, J., S. Schorr, …, D. M. Lilley. 2011. Orientation of cyanine fluorophores terminally attached to DNA via long, flexible tethers. *Biophys. J.* 101:1148–1154.
25. Van der Meer, B. W. 1999. Orientational Aspects in Pair Energy Transfer. John Wiley & Sons, Ltd., London.
26. Dale, R. E., and J. Eisinger. 1976. Intramolecular energy transfer and molecular conformation. *Proc. Natl. Acad. Sci. USA.* 73:271–273.
27. Loura, L. M. 2012. Simple estimation of Forster resonance energy transfer (FRET) orientation factor distribution in membranes. *Int. J. Mol. Sci.* 13:15252–15270.
28. Hoefling, M., and H. Grubmuller. 2013. In silico FRET from simulated dye dynamics. *Comput. Phys. Commun.* 184:841–852.
29. VanBeek, D. B., M. C. Zwier, …, B. P. Krueger. 2007. Fretting about FRET: correlation between kappa and R. *Biophys. J.* 92:4168–4178.
30. Ranjit, S., K. Gurunathan, and M. Levitus. 2009. Photophysics of backbone fluorescent DNA modifications: reducing uncertainties in FRET. *J. Phys. Chem. B.* 113:7861–7866.
31. Ivanov, V., M. Li, and K. Mizuuchi. 2009. Impact of emission anisotropy on fluorescence spectroscopy and FRET distance measurements. *Biophys. J.* 97:922–929.
32. Rothwell, P. J., S. Berger, …, C. A. Seidel. 2003. Multiparameter single-molecule fluorescence spectroscopy reveals heterogeneity of HIV-1 reverse transcriptase:primer/template complexes. *Proc. Natl. Acad. Sci. USA.* 100:1655–1660.
33. Sindbert, S., S. Kalinin, …, C. A. Seidel. 2011. Accurate distance determination of nucleic acids via Förster resonance energy transfer: implications of dye linker length and rigidity. *J. Am. Chem. Soc.* 133:2463–2480.
34. Muschielok, A., J. Andrecka, …, J. Michaelis. 2008. A nano-positioning system for macromolecular structural analysis. *Nat. Methods.* 5:965–971.
35. Muschielok, A., and J. Michaelis. 2011. Application of the nano-positioning system to the analysis of fluorescence resonance energy transfer networks. *J. Phys. Chem. B.* 115:11927–11937.
36. Milas, P., B. D. Gamari, …, L. S. Goldner. 2013. Indocyanine dyes approach free rotation at the 3′ terminus of A-RNA: a comparison with the 5′ terminus and consequences for fluorescence resonance energy transfer. *J. Phys. Chem. B.* 117:8649–8658.
37. Spiriti, J., J. K. Binder, …, A. van der Vaart. 2011. Cy3-DNA stacking interactions strongly depend on the identity of the terminal basepair. *Biophys. J.* 100:1049–1057.
38. Corry, B., and D. Jayatilaka. 2008. Simulation of structure, orientation, and energy transfer between AlexaFluor molecules attached to MscL. *Biophys. J.* 95:2711–2721.
39. Iqbal, A., S. Arslan, …, D. M. Lilley. 2008. Orientation dependence in fluorescent energy transfer between Cy3 and Cy5 terminally attached to double-stranded nucleic acids. *Proc. Natl. Acad. Sci. USA.* 105: 11176–11181.
40. Deplazes, E., D. Jayatilaka, and B. Corry. 2011. Testing the use of molecular dynamics to simulate fluorophore motions and FRET. *Phys. Chem. Chem. Phys.* 13:11045–11054.

41. Hoefling, M., N. Lima, …, H. Grubmüller. 2011. Structural heterogeneity and quantitative FRET efficiency distributions of polyprolines through a hybrid atomistic simulation and Monte Carlo approach. *PLoS ONE.* 6:e19791.

42. Shoura, M. J., A. A. Vetcher, …, S. D. Levene. 2012. Measurements of DNA-loop formation via Cre-mediated recombination. *Nucleic Acids Res.* 40:7452–7464.

43. Zarrabi, N., S. Ernst, …, M. Börsch. 2014. Analyzing conformational dynamics of single P-glycoprotein transporters by Förster resonance energy transfer using hidden Markov models. *Methods.* 66:168–179.

44. Thévenin, D., and T. Lazarova. 2012. Identifying and measuring transmembrane helix-helix interactions by FRET. *Methods Mol. Biol.* 914:87–106.

45. Guo, F., D. N. Gopaul, and G. D. van Duyne. 1997. Structure of Cre recombinase complexed with DNA in a site-specific recombination synapse. *Nature.* 389:40–46.

46. Guo, F., D. N. Gopaul, and G. D. Van Duyne. 1999. Asymmetric DNA bending in the Cre-loxP site-specific recombination synapse. *Proc. Natl. Acad. Sci. USA.* 96:7143–7148.

47. Phillips, J. C., R. Braun, …, K. Schulten. 2005. Scalable molecular dynamics with NAMD. *J. Comput. Chem.* 26:1781–1802.

48. MacKerell, Jr., A. D., N. Banavali, and N. Foloppe. 2000-2001. Development and current status of the CHARMM force field for nucleic acids. *Biopolymers.* 56:257–265.

49. Hoover, W. G. 1985. Canonical dynamics: equilibrium phase-space distributions. *Phys. Rev. A.* 31:1695–1697.

50. Flyvbjerg, H., and H. Petersen. 1989. Error estimates on average of correlated data. *J. Chem. Phys.* 91:461–466.

51. Hill, T. L. 1956. Statistical Mechanics. Principles and Selected Applications. McGraw Hill, New York.

52. Lopes, P. E. M., B. Roux, and A. D. Mackerell, Jr. 2009. Molecular modeling and dynamics studies with explicit inclusion of electronic polarizability. Theory and applications. *Theor. Chem. Acc.* 124:11–28.

53. Lin, H., and D. Truhlar. 2007. QM/MM: what have we learned, where are we, and where do we go from here? *Theor. Chem. Acc.* 177: 185–199.

54. Egorov, A. V., A. P. Lyubartsev, and A. Laaksonen. 2011. Molecular dynamics simulation study of glycerol-water liquid mixtures. *J. Phys. Chem. B.* 115:14572–14581.

55. Ringrose, L., V. Lounnas, …, A. F. Stewart. 1998. Comparative kinetic analysis of FLP and cre recombinases: mathematical models for DNA binding and recombination. *J. Mol. Biol.* 284:363–384.

56. Shankar, P. N., and M. Kumar. 1994. Experimental Determination of the Kinematic Viscosity of Glycerol-Water Mixtures. *Proc. R. Soc. Lond., A.* 444:573–581.

57. Speelman, A. L., A. Muñoz-Losa, …, B. P. Krueger. 2011. Using molecular dynamics and quantum mechanics calculations to model fluorescence observables. *J. Phys. Chem. A.* 115:3997–4008.

58. Lee, L., and P. D. Sadowski. 2003. Identification of Cre residues involved in synapsis, isomerization, and catalysis. *J. Biol. Chem.* 278:36905–36915.

59. Vetcher, A. A., A. Y. Lushnikov, …, S. D. Levene. 2006. DNA topology and geometry in Flp and Cre recombination. *J. Mol. Biol.* 357:1089–1104.

60. Gopaul, D. N., F. Guo, and G. D. Van Duyne. 1998. Structure of the Holliday junction intermediate in Cre-loxP site-specific recombination. *EMBO J.* 17:4175–4187.

CONTRIBUTION OF FLUOROPHORE DYNAMICS AND SOLVATION TO RESONANT ENERGY TRANSFER IN PROTEIN-DNA COMPLEXES: A MOLECULAR-DYNAMICS STUDY

Massa J. Shoura,[1,2] R. J. K. Udayana Ranatunga,[3] Sarah A. Harris,[5] Steven O. Nielsen,[3] and Stephen D. Levene [1,2,4,*]

[1]Departments of Bioengineering, [2]Molecular and Cell Biology, [3]Chemistry, and [4]Physics
University of Texas at Dallas
800 West Campbell Road
Richardson, TX 75080
USA

[5]Department of Physics and Astronomy
University of Leeds
E.C. Stoner Building
Leeds LS2 9JT
United Kingdom

Supporting Material

Table S1: List of systems simulated in this work

System	Trajectory duration, ns
DNA duplex in water	W/O ATTO dyes: **46** W/ ATTO dyes: **58**
DNA- Cre synapsis (5CRX) in water	W/O ATTO dyes: **49** W/ ATTO dyes parallel: **57** W/ ATTO dyes antiparallel: **58**
DNA Holiday junction without Cre in water	W/O ATTO dyes: **60** W/ ATTO dyes scenario (I) : **56** W/ ATTO dyes scenario (II): **51**
DNA-Cre Holiday junction (3CRX) in water	W/O ATTO dyes: **45** W/ ATTO dyes scenario (I) : **54** W/ ATTO dyes scenario (II): **57**
DNA-Cre Holiday junction (3CRX) in water:glycerol	W/ ATTO dyes scenario (II): **200**
Controls- Tethered dyes in water	d= 2 nm: **30** d= 3 nm: **30** d= 4 nm: **30** d= 5 nm: **30** d= 7.3 nm: **30**
Controls- Tethered dyes in water:glycerol	d= 2 nm: **100** d= 4 nm: **110** d= 7.3 nm: **100**

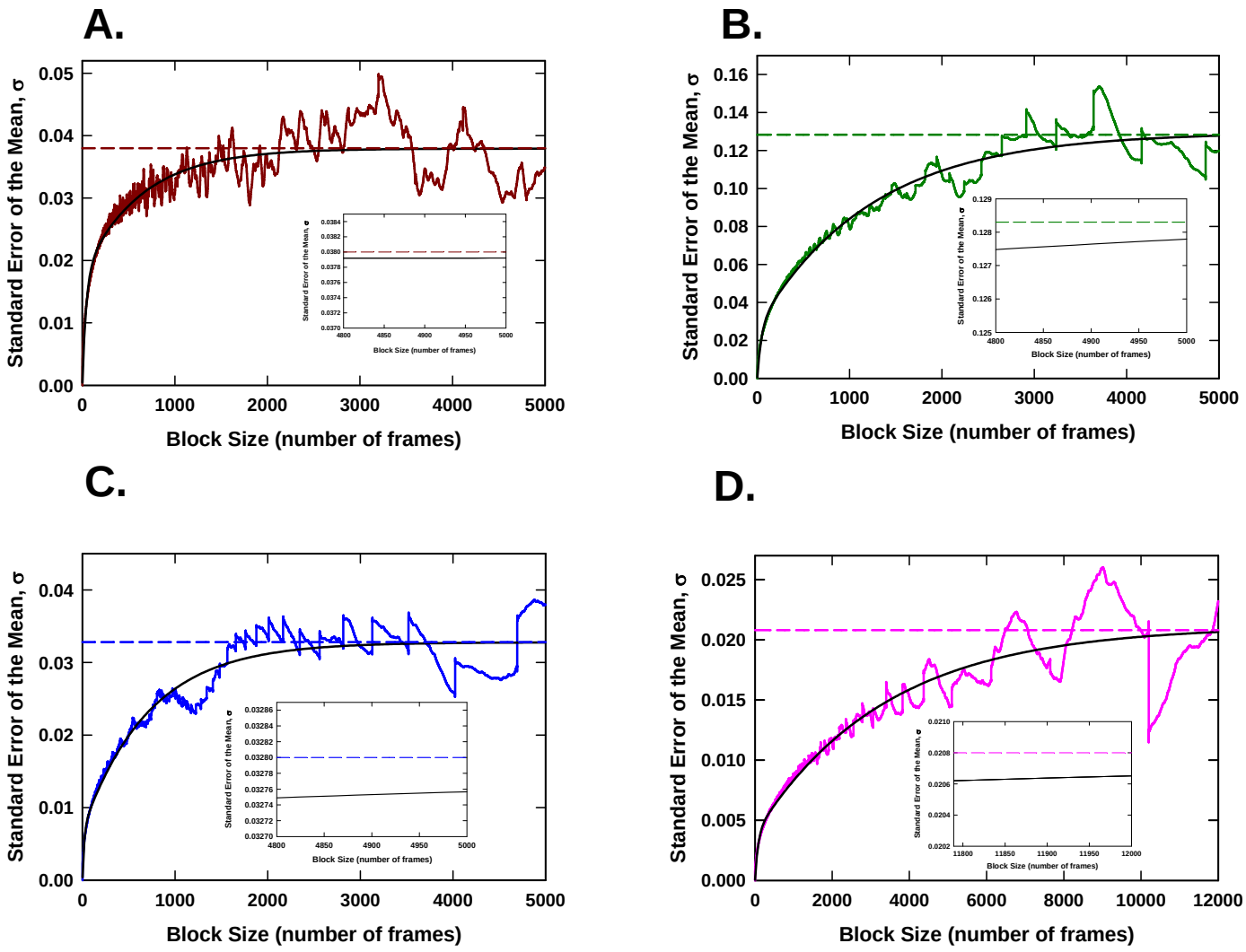

Figure S1. Block-averaging analysis of MD trajectories for convergence and statistical noise. The solid black lines show a mono- or bi-exponential fit to the apparent standard error, σ, in $\langle\kappa^2(t)\rangle_T$ as a function of data-block size. The dashed line gives the asymptotic value of the exponential fit, σ*, which corresponds to an estimated lower bound for the standard error in $\langle\kappa^2(t)\rangle_T$ over the full trajectory. Corresponding systems are: (A.) DNA duplex (system (ii.)), (B.) antiparallel Cre-DNA synaptic complex (system (iii.)), (C.) and (D.) Cre-DNA Holliday-junction intermediate (system (iv.)) in water; and glycerol:water, respectively. Insets show the respective approaches of the fitted dependencies to their asymptotic values in the limit of large block size. The fitted values for maximum block size and corresponding asymptotic values are similar at the 1% level; although this suggests sufficient equilibration of $\langle\kappa^2(t)\rangle_T$ to support the conclusions of this study, these trajectories are likely not long enough to supply an upper bound for σ*.

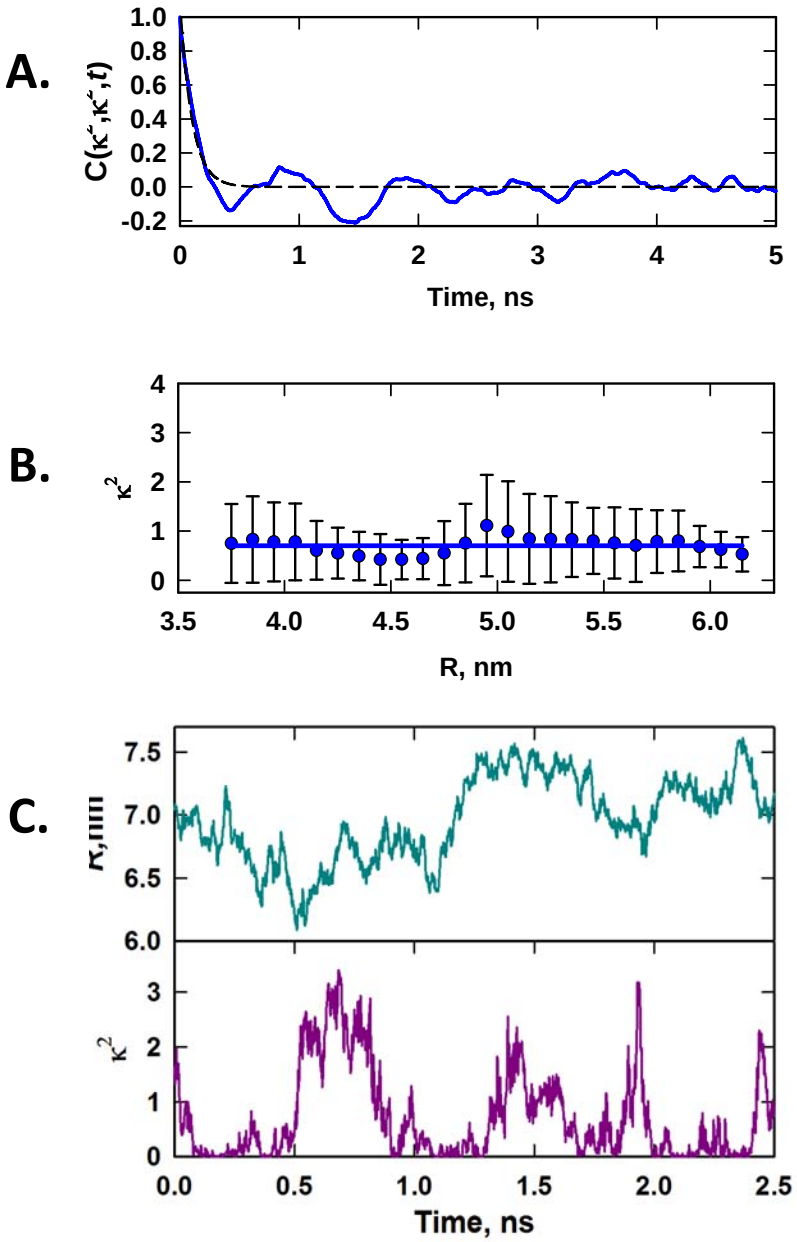

Figure S2. Dynamics of tethered ATTO dyes with *d* = 5 nm; total trajectory duration was 30 ns. **(A.)** The autocorrelation function for κ^2, $C(\kappa^2,\kappa^2;\tau) = <\kappa^2(t)\kappa^2(t+\tau)>_T$ (solid blue line) with a single-exponential fit (dashed black line). The decay time τ of the fit is 100 ps. **(B.)** Binned scatter plot of κ^2 as a function of *R* for the tethered dyes. The average value of κ^2 is 0.65, shown as a solid blue line. **(C.)** Time-dependent fluctuations of the orientation factor, κ^2 and center-of-mass distance between the dyes, *R*.

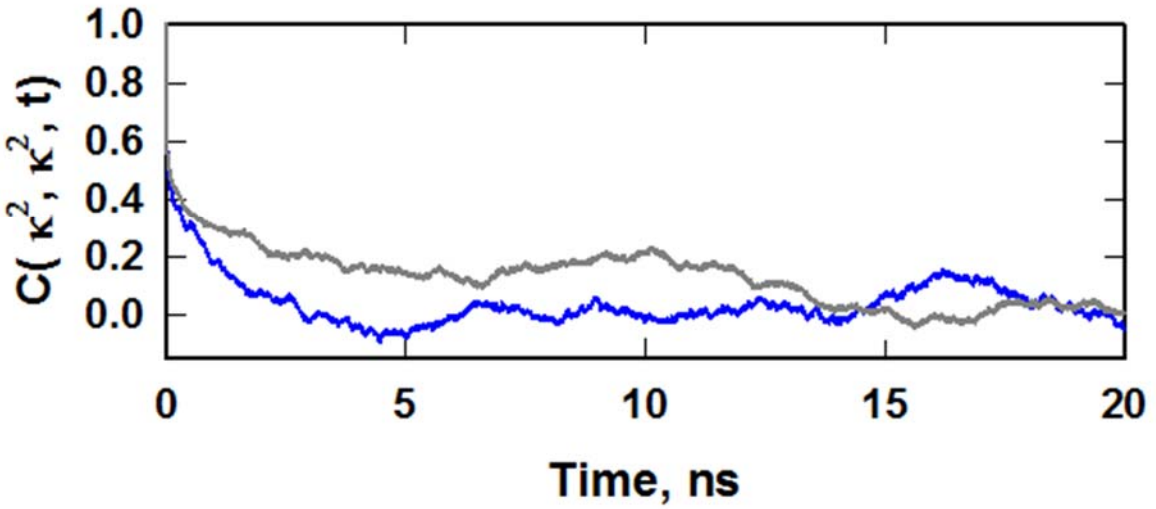

Figure S3. Dynamics of ATTO dyes conjugated to a Cre-DNA holliday junction complex. The autocorrelation function for κ^2, $C(\kappa^2,\kappa^2;\tau) = <\kappa^2(t)\kappa^2(t+\tau)>_T$ is shown for system (iv.) in water (blue) and glycerol:water (grey). We estimate decay times of 1 ns (aqueous) and 9 ns (glycerol:water). MD trajectories for the Cre-HJ complex in water and glycerol:water were carried out for times that are more than 20 times the respective autocorrelation-decay times for κ^2.

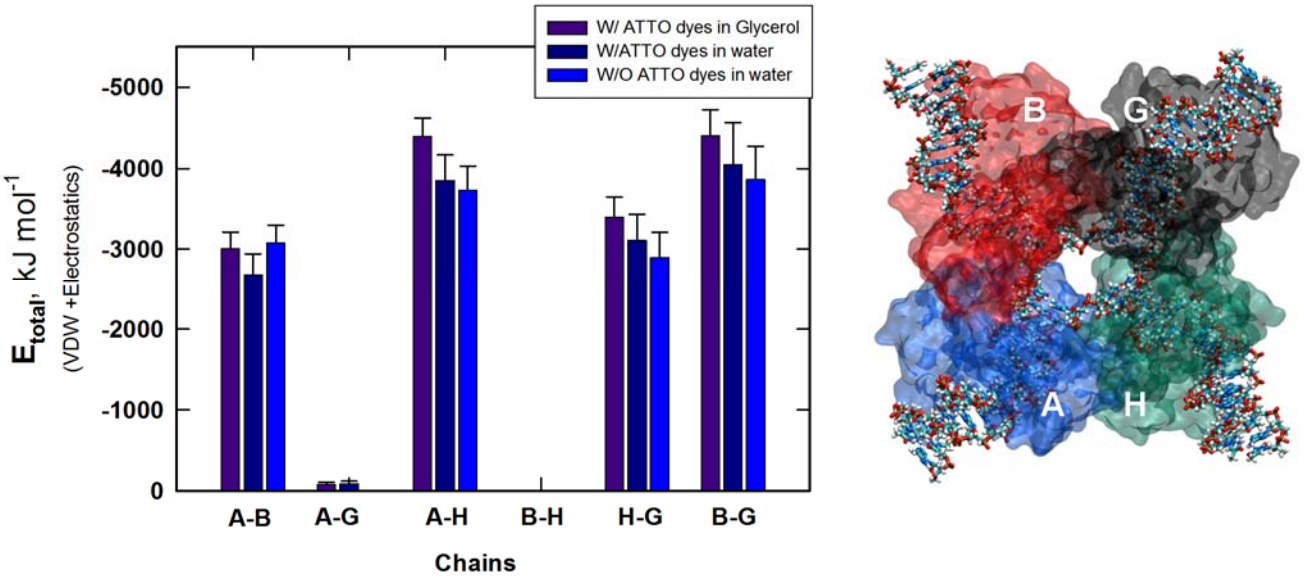

Figure S4. Stabilization energy of the 3CRX Cre-HJ complex. The sum of van der Waals and electrostatic components of the potential energy of interaction between Cre monomers, labeled A, B, G, and H. All energetic contributions from DNA binding, as well as DNA-DNA interactions, are excluded. Note that incorporation of ATTO dyes does not affect the stability of the complex in water. There is a small, but measurable, stabilization of protein-protein interactions in glycerol-water mixture.

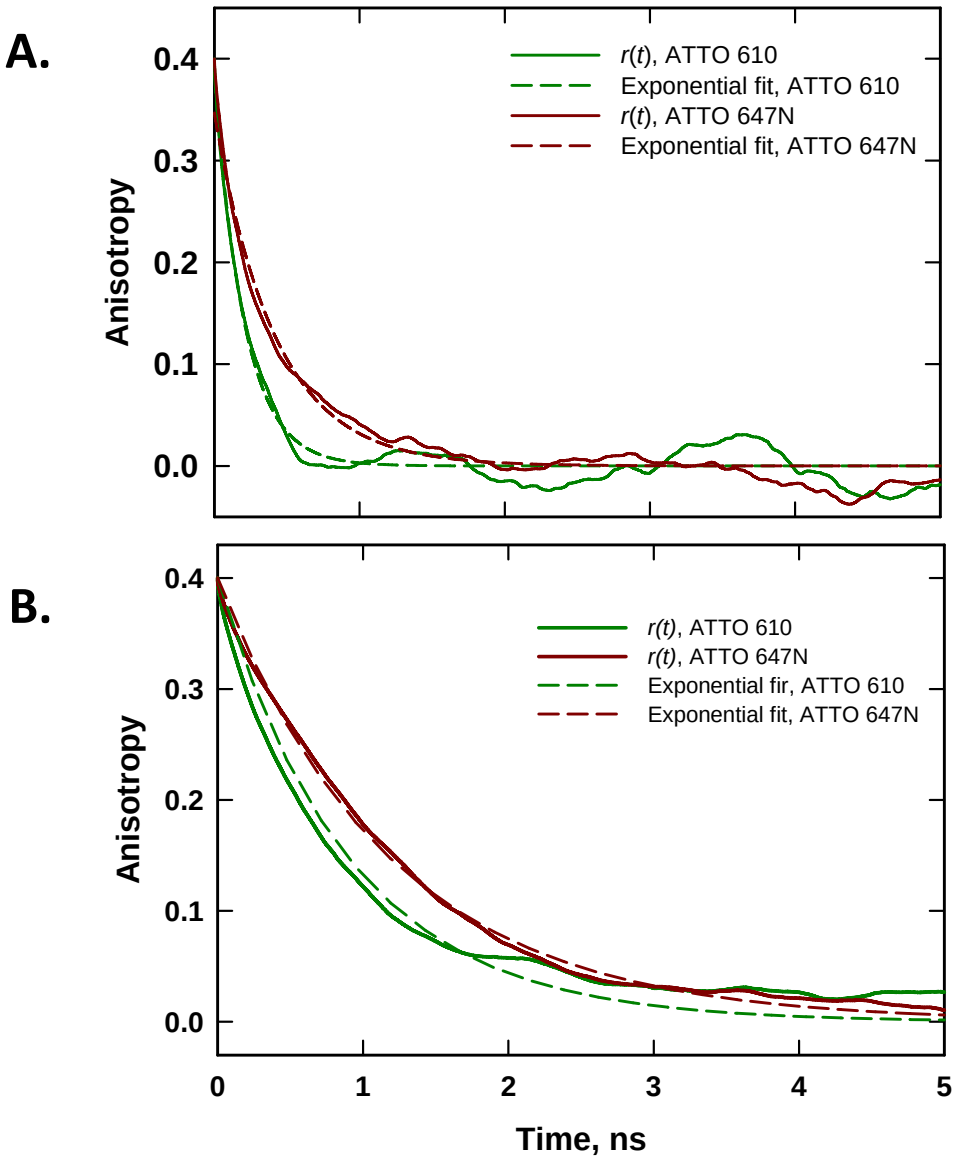

Figure S5. Time-dependent anisotropy, $r(t)$, of individual ATTO dyes**. (A.)** Simulations in aqueous-solvent conditions. Single-exponential fits yielded correlation times of 400 and 640 ps for ATTO 610 and ATTO 647N, respectively. The smaller value attributed to ATTO 610 is expected due to the smaller dimensions of the fluorophore. **(B)** Simulations in water:glycerol solvent yielded correlation times of 1.2 and 1.7 ns for ATTO 610 and ATTO 647N, respectively. The relative time constants for water:glycerol mixtures and aqueous solvent are quantitatively consistent with the increment in bulk solvent viscosity.

Appendix: Topology Files for ATTO 647N and ATTO 610 (CHARMM Format)

```
!!!!!!!!!!!!!!!!!!!!!!!!!!!!!!!!!!!!!!!!!!!!!!!!!!!!!!!!!!!!!!!!!!!!!!!
!!!! ATTO Dyes Topology file By: Massa Shoura and Udy Ranatunga 2013!!!!
!!!!!!!!!!!!!!!!!!!!!!!!!!!!!!!!!!!!!!!!!!!!!!!!!!!!!!!!!!!!!!!!!!!!!!!
!!!!!!!!!!!!!!!!!!!!!!!!!!!!!!!!!!!!!!!!!!!!!!
!!!!!!!! ATTO 647N Dye molecule topology!!!!!!!!
!!!!!!!!!!!!!!!!!!!!!!!!!!!!!!!!!!!!!!!!!!!!!!

RESI A647         +1.00 !

!N and adjacent C
GROUP
ATOM C34  CA      0.000 !
GROUP
ATOM C41  CA     -0.115 !
ATOM H25  HP      0.115 !
GROUP
ATOM C40  CA      0.000 !
GROUP
ATOM C35  CA     -0.115 !
ATOM H41  HP      0.115 !
GROUP                   !
ATOM C39  CT2    -0.18  !
ATOM H27  HA      0.09  !
ATOM H26  HA      0.09  !
GROUP                   !
ATOM C38  CT2    -0.18  !
ATOM H29  HA      0.09  !
ATOM H28  HA      0.09  !

!delocalized N group
GROUP
! 1st N and its neighbors
ATOM N4   N3R    -0.506 !         ESP charge optimized
ATOM C37  CT      0.558 !         ESP charge optimized
ATOM C46  CT2     0.147 !         ESP charge optimized
ATOM H40  HA      0.09  !
ATOM H42  HA      0.09  !
ATOM C36  CA      0.434 !         ESP charge optimized
! 2nd N+ and its neighbors
ATOM N5   NRA    -0.067 !         ESP charge optimized
ATOM C27  CT2     0.030 !         ESP charge optimized
ATOM H52  HA      0.09  !
ATOM H53  HA      0.09  !
ATOM C43  CA      0.077 !         ESP charge optimized
ATOM C28  CT2    -0.223 !         ESP charge optimized
ATOM H54  HA      0.09  !
ATOM H55  HA      0.09  !

GROUP                   !
ATOM C49  CT3    -0.27  !
ATOM H31  HA      0.09  !
ATOM H32  HA      0.09  !
```

```
ATOM H33  HA      0.09  !
GROUP                   !
ATOM C48  CT3    -0.27  !
ATOM H34  HA      0.09  !
ATOM H35  HA      0.09  !
ATOM H36  HA      0.09  !
GROUP                   !
ATOM C47  CT3    -0.27  !
ATOM H37  HA      0.09  !
ATOM H38  HA      0.09  !
ATOM H39  HA      0.09  !

!RING
GROUP                   !
ATOM C26  CE1    -0.15  !
ATOM C25  CE1    -0.15  !
ATOM H51  HE1     0.15  !
ATOM H50  HE1     0.15  !

!RING
GROUP                   !
ATOM C30  CT2    -0.18  !
ATOM H59  HA      0.09  !
ATOM H58  HA      0.09  !
GROUP                   !
ATOM C29 CT2     -0.18  !
ATOM H56  HA      0.09  !
ATOM H57  HA      0.09  !

!RING
GROUP                   !
ATOM C23  CA     -0.115 !
ATOM H49  HP      0.115 !
GROUP                   !
ATOM C24  CA      0.000 !
GROUP                   !
ATOM C31  CA      0.000 !
!RING
GROUP                   !
ATOM C42  CA      0.000 !
GROUP                   !
ATOM C33  CT      0.000 !
GROUP                   !
ATOM C32  CA      0.000 !
GROUP                   !
ATOM C22  CA      0.000 !
GROUP                   !
ATOM C21  CA      0.000 !
GROUP                   !
ATOM C44  CT3    -0.27  !
ATOM H46  HA      0.09  !
ATOM H47  HA      0.09  !
ATOM H48  HA      0.09  !
GROUP                   !
```

```
ATOM C45  CT3    -0.27  !
ATOM H43  HA      0.09  !
ATOM H44  HA      0.09  !
ATOM H45  HA      0.09  !

!RING
GROUP                   !
ATOM C16  CA     -0.115 !
ATOM H20  HP      0.115 !
GROUP                   !
ATOM C17  CA     -0.115 !
ATOM H21  HP      0.115 !
GROUP                   !
ATOM C18  CA     -0.115 !
ATOM H22  HP      0.115 !
GROUP                   !
ATOM C19  CA     -0.115 !
ATOM H23  HP      0.115 !
GROUP                   !
ATOM C15  CA      0.000 !
GROUP                   !
ATOM C20  CA      0.000 !
GROUP                   !
ATOM C14  CC      0.55  !
ATOM O3   O      -0.55  !
GROUP                   !
ATOM N3   N      -0.29  ! -PRO
!ATOM HN3  H      0.31  !  |
ATOM C50    CT3        0.02  !  |
ATOM H60    HA         0.09  !  |
ATOM H61    HA         0.09  !  |
ATOM H62  HA           0.09  !  /
GROUP
ATOM C13  CT2    -0.18  !
ATOM H18  HA      0.09  !
ATOM H19  HA      0.09  !

! BUTANAL PENDANT
GROUP                   !
ATOM C12  CT2    -0.18  !
ATOM H16  HA      0.09  !
ATOM H17  HA      0.09  !
GROUP                   !
ATOM C11  CT2    -0.18  !
ATOM H24  HA      0.09  !
ATOM H15  HA      0.09  !
GROUP                   !
ATOM C10  CC      0.55  !
ATOM O2   O      -0.55  !

!LINKER
GROUP                   !
ATOM N2   NH2    -0.47  ! -ALAD residue
ATOM HN2  H       0.31  !  |
```

```
ATOM C9   CT2    -0.02  !  |
ATOM H14  HA      0.09  !  |
ATOM H13  HA      0.09  ! _/
GROUP                   !
ATOM C8   CT2    -0.18  !
ATOM H11  HA      0.09  !
ATOM H12  HA      0.09  !
GROUP                   !
ATOM C7   CT2    -0.18  !
ATOM H9   HA      0.09  !
ATOM H10  HA      0.09  !
GROUP                   !
ATOM C6   CT2    -0.18  !
ATOM H7   HA      0.09  !
ATOM H8   HA      0.09  !
GROUP                   !
ATOM C5   CT2    -0.18  !
ATOM H5   HA      0.09  !
ATOM H6   HA      0.09  !
GROUP                   !
ATOM C4   CT2    -0.01  ! -ALAD residue
ATOM H3   HA      0.09  !  |
ATOM H4   HA      0.09  !  |
ATOM N1   NH2    -0.47  !  |
ATOM HN1  H       0.31  ! _/
GROUP                   !
ATOM C3   CC      0.55  !
ATOM O1   O      -0.55  !
GROUP                   !
ATOM C1  CE1     -0.15  ! -PRPE residues
ATOM C2  CE1     -0.15  !  |
ATOM H1  HE1      0.15  !  |
ATOM H2  HE1      0.15  ! _/

DOUBLE C1 C2                                            !
DOUBLE C3 O1                                            !
DOUBLE C14 O3                                           !
DOUBLE C10 O2                                           !

BOND C1  H1                                             !
BOND C2  H2                                             !
BOND C2  C3  C3  N1  N1  HN1 N1  C4  C4  H3 C4 H4       !
BOND C4  C5  C5  H5  C5  H6  C5  C6  C6  H7 C6 H8       !
!BOND C7  C6  C7  H9  C7  H10 C7  C8  H11 C8 H12      !
!BOND C8  C9  C9  N2  N2  HN2 N2  C10                 !
BOND C6  C7  C7  C8  C8  C9  C9  N2  N2  C10          !
BOND C7  H9  C7  H10
BOND N2  HN2 C8  H11 C8  H12 C9  H13 C9  H14          !
BOND C10 C11 C11 H24 C11 H15 C11 C12 C12 H16 C12 H17     !
BOND C12 C13 C13 H18 C13 H19 C13 N3  N3  C50 N3 C14   !
BOND C50 H60 C50 H61 C50 H62                                    !
BOND C14 C15 C15 C16 C16 H20 C16 C17 C17 H21 C17 C18     !
BOND C18 H22 C18 C19 C19 H23 C19 C20 C20 C15 C20 C21     !
BOND C21 C22 C22 C23 C23 H49 C23 C24 C24 C43 C43 C31     !
```

```
BOND C31 C32 C32 C22   C21 C42 C42 C34 C34 C33 C33 C32    !
BOND C33 C45 C33 C44
                      !
BOND C45 H43 C45 H44 C45 H45 C44 H46 C44 H47 C44 H48     !
BOND C24 C25 C25 H50 C25 C26 C26 H51 C26 C27                    !
BOND C27 H52 C27 H53 C27 N5  N5  C28 N5  C43          !
BOND C28 H54 C28 H55 C28 C29
      !
BOND C29 H56 C29 H57 C29 C30
      !
BOND C30 H58 C30 H59 C30 C31
      !
BOND C47 H37 C47 H38 C47 H39 C47 C46
BOND C46 H42 C46 H40 C46 N4  N4  C37
BOND C48 H34 C48 H35 C48 H36 C48 C37
BOND C49 H31 C49 H32 C49 H33 C49 C37
BOND C38 H28 C38 H29 C37 C38 C38 C39
BOND C39 H26 C39 H27 C39 C40 C40 C36
BOND C36 N4  C36 C35 C35 H41 C35 C34
BOND C41 C40 C41 C42 C41 H25


PRES LNK2        -0.00   ! patch for linking ATTO 647N to THY C5M
                                                !
GROUP                          !
ATOM 2N1   NN2B   -0.34  !
ATOM 2C6   CN3     0.17  !
ATOM 2H6   HN3     0.17  !
ATOM 2C2   CN1T    0.51  !
ATOM 2O2   ON1    -0.41  !
ATOM 2N3   NN2U   -0.46  !
ATOM 2H3   HN2     0.36  !
ATOM 2C4   CN1     0.50  !
ATOM 2O4   ON1    -0.45  !
ATOM 2C5   CN3T   -0.15  !
ATOM 2C5M  CN9    -0.04  !
ATOM 2H52  HN9     0.07  !
ATOM 2H53  HN9     0.07  !
BOND 1C1   2C5M
DELETE ATOM 2H51

!!!!!!!!!!!!!!!!!!!!!!!!!!!!!!!!!!!!!!!!!!!!!!!!!!
!!!!!!!! ATTO 610 Dye molecule topology!!!!!!!!!
!!!!!!!!!!!!!!!!!!!!!!!!!!!!!!!!!!!!!!!!!!!!!!!!!!

RESI A610        +1.00  ! topology of ATTO-610 dye
                        ! Massa Shoura Oct 21st 2011
                                              ! updated, June 27, 2012 MS
!N and adjacent C
GROUP
ATOM C19  CT3    -0.161 ! -0.171 ! ESP charge optimized
ATOM H13  HA      0.09  !
ATOM H14  HA      0.09  !
ATOM H15  HA      0.09  !
```

```
ATOM C18  CT3    -0.179 ! -0.189 ! ESP charge optimized
ATOM H10  HA      0.09  !
ATOM H11  HA      0.09  !
ATOM H12  HA      0.09  !
ATOM N1   NRA    -0.090 ! -0.100 ! ESP charge optimized
ATOM C15  CA      0.497 !  0.487 ! ESP charge optimized
ATOM C3   CA      0.333 !  0.323 ! ESP charge optimized
ATOM N2   N3R    -0.044 ! -0.054 ! ESP charge optimized
ATOM C7   CT2    -0.060 ! -0.070 ! ESP charge optimized
ATOM H39  HA      0.09  !
ATOM H5   HA      0.09  !
ATOM C20  CT2    -0.206 ! -0.23  ! ESP charge optimized
ATOM H16  HA      0.09  !
ATOM H17  HA      0.09  !

GROUP                   !
ATOM C16  CA     -0.115 !
ATOM H8   HP      0.115 !
GROUP                   !
ATOM C17  CA     -0.115 !
ATOM H9   HP      0.115 !
GROUP                   !
ATOM C14  CA     -0.115 !
ATOM H7   HP      0.115 !
GROUP                   !
ATOM C12  CA      0.000 !
GROUP                   !
ATOM C13  CA      0.000 !

! RING 2
GROUP                   !
ATOM C34  CT3    -0.27  !
ATOM H44  HA      0.09  !
ATOM H45  HA      0.09  !
ATOM H46  HA      0.09  !
GROUP                   !
ATOM C33  CT3    -0.27  !
ATOM H41  HA      0.09  !
ATOM H42  HA      0.09  !
ATOM H43  HA      0.09  !
GROUP                   !
ATOM C10  CT      0.00  !
GROUP                   !
ATOM C11  CA     -0.115 !
ATOM H6   HP      0.115 !
GROUP                   !
ATOM C8   CA      0.000 !
GROUP                   !
ATOM C9   CA      0.000 !

!RING 3
GROUP                   !
ATOM C1 CA       -0.115 !
ATOM H1 HP        0.115 !
```

```
GROUP                   !
ATOM C2 CA       -0.115 !
ATOM H2 HP        0.115 !
GROUP                   !
ATOM C4 CA        0.000 !

!RING 4
GROUP
ATOM C5   CT2    -0.18  !
ATOM H3   HA      0.09  !
ATOM H40  HA      0.09  !
GROUP                   !
ATOM C6   CT2    -0.18  !
ATOM H4   HA      0.09  !
ATOM H38  HA      0.09  !

! BUTANAL PENDANT
GROUP                   !
ATOM C21  CT2    -0.18  !
ATOM H18  HA      0.09  !
ATOM H19  HA      0.09  !
GROUP                   !
ATOM C22  CT2    -0.18  !
ATOM H20  HA      0.09  !
ATOM H21  HA      0.09  !
GROUP                   !
ATOM C23  CC      0.55  !
ATOM O1   O      -0.55  !

! LINKER
GROUP                   !
ATOM N3   NH2    -0.47  ! -ALAD residue
ATOM H22  H       0.31  !  |
ATOM C24  CT2    -0.02  !  |
ATOM H23  HA      0.09  !  |
ATOM H24  HA      0.09  ! _/
GROUP                   !
ATOM C25  CT2    -0.18  !
ATOM H25  HA      0.09  !
ATOM H26  HA      0.09  !
GROUP                   !
ATOM C26  CT2    -0.18  !
ATOM H27  HA      0.09  !
ATOM H28  HA      0.09  !
GROUP                   !
ATOM C27  CT2    -0.18  !
ATOM H29  HA      0.09  !
ATOM H30  HA      0.09  !
GROUP                   !
ATOM C28  CT2    -0.18  !
ATOM H31  HA      0.09  !
ATOM H32  HA      0.09  !
GROUP                   !
ATOM C29  CT2    -0.01  ! -ALAD residue
```

```
ATOM H33  HA      0.09  !  |
ATOM H34  HA      0.09  !  |
ATOM N4   NH2    -0.47  !  |
ATOM H35  H       0.31  ! _/
GROUP                   !
ATOM C30  CC      0.55  !
ATOM O2   O      -0.55  !
GROUP                   !
ATOM C31  CE1    -0.15  ! -PRPE residues
ATOM C32  CE1    -0.15  !  |
ATOM H36  HE1     0.15  !  |
ATOM H37  HE1     0.15  ! _/

BOND N1  C18 N1  C19                                   !
DOUBLE N1 C15                                          !
BOND C19 H13 C19 H14 C19 H15 C18 H10 C18 H11 C18 H12 !
BOND C15 C16 C16 C17 C17 C12 C12 C13 C13 C14 C14 C15 ! RING 1 CARBONS
BOND C14 H7  C16 H8  C17 H9                          ! RING 1 Hs
BOND C12 C11 C11 C8  C8  C9  C9  C10 C10 C13         ! RING 2 CARBONS
BOND C11 H6  C10 C33 C10 C34                         ! RING 2 SUBS
BOND C34 H44 C34 H45 C34 H46 C33 H41 C33 H42 C33 H43 !   "  "  "
BOND C8  C1  C1  C4  C4  C3  C3  C2  C2  C9          ! RING 3 CARBONS
BOND C1  H1  C2  H2                                  ! RING 3 Hs
BOND C4  C5  C5  C6  C6  C7  C7  N2  N2  C3          ! RING 4 CARBONS/N
BOND C5  H3  C5  H40 C6  H4  C6  H38 C7  H39 C7 H5   ! RING 4 Hs
BOND N2  C20 C20 H16 C20 H17 C20 C21                 !
BOND C21 H18 C21 H19 C21 C22 C22 H20 C22 H21         !
BOND C22 C23 C23 N3  N3  H22 N3  C24                 !
DOUBLE   C23 O1                                      !
BOND C24 H23 C24 H24 C24 C25 C25 H25 C25 H26 C25 C26 !
BOND C26 H27 C26 H28 C26 C27 C27 H29 C27 H30 C27 C28 !
BOND C28 H31 C28 H32 C28 C29 C29 H33 C29 H34 C29 N4  !
BOND N4  H35 N4  C30 C30 C31 C31 H36 C32 H37         !
DOUBLE   C30 O2  C31 C32                             !

PRES LNK1         -0.00  ! patch for linking ATTO 610 to THY C5M
                                                   !
GROUP                          !
ATOM 2N1   NN2B   -0.34  !
ATOM 2C6   CN3     0.17  !
ATOM 2H6   HN3     0.17  !
ATOM 2C2   CN1T    0.51  !
ATOM 2O2   ON1    -0.41  !
ATOM 2N3   NN2U   -0.46  !
ATOM 2H3   HN2     0.36  !
ATOM 2C4   CN1     0.50  !
ATOM 2O4   ON1    -0.45  !
ATOM 2C5   CN3T   -0.15  !
ATOM 2C5M  CN9    -0.04  !
ATOM 2H52  HN9     0.07  !
ATOM 2H53  HN9     0.07  !
BOND 1C32  2C5M
DELETE ATOM 2H51
```
!!!!!!!!!!!!!!!!!!!!!!!!!!!!!!!!The End!!!!!!!!!!!!!!!!!!!!!!!!!!!!!!!!